

Detecting Persuasive Atypicality by Modeling Contextual Compatibility

Meiqi Guo Rebecca Hwa Adriana Kovashka

Department of Computer Science, University of Pittsburgh, Pittsburgh PA, USA

meiqi.guo@pitt.edu {hwa, kovashka}@cs.pitt.edu

<https://github.com/MeiqiGuo/ICCV2021-AtypicalityDetection>

Abstract

We propose a new approach to detect atypicality in persuasive imagery. Unlike atypicality which has been studied in prior work, persuasive atypicality has a particular purpose to convey meaning, and relies on understanding the common-sense spatial relations of objects. We propose a self-supervised attention-based technique which captures contextual compatibility, and models spatial relations in a precise manner. We further experiment with capturing common sense through the semantics of co-occurring object classes. We verify our approach on a dataset of atypicality in visual advertisements, as well as a second dataset capturing atypicality that has no persuasive intent.

1. Introduction

Visually creative images, such as advertisements or public service announcements, may purposefully contain atypical portrayals of objects as a rhetorical way for attracting viewers’ attention [15]. In the marketing and communications research community, atypicality has gained attention because of its importance to understanding the persuasiveness and rhetoric of visual media [28, 23, 48]. However, detecting this type of atypicality is challenging for intelligent systems. First, atypicality may involve metaphorical object transformations or intentionally surprising composed objects. Second, the atypicality transformation types are diverse and creative. Third, unpacking them may require common-sense reasoning. For example, Fig. 1a is an atypical advertisement for a beverage. It is unusual for a pig to wear a bridal veil even though the pig and veil are both normal objects. The ability to detect this type of purposefully atypical objects and understand their roles in conveying the intent of the image is necessary for an intelligent system to reason about information in persuasive media. In this work, we propose to model implicit knowledge of contextual compatibility in order to detect *persuasive atypicality*.

Our first hypothesis is that persuasive atypicality can be detected by checking the compatibility between each possibly atypical object and the rest of the image as context.

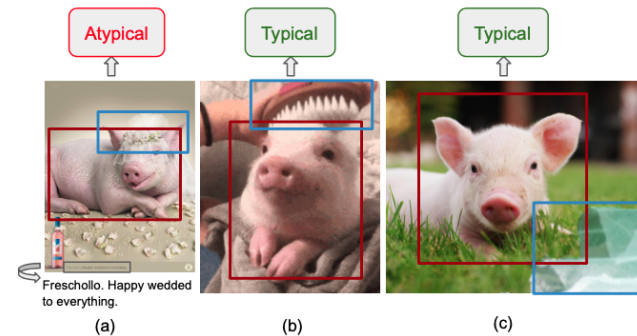


Figure 1. These images illustrate the importance of object interactions and their spatial relative position for atypicality detection. (a) Pig wearing a bridal veil is atypical; (b) If a handled brush instead of a veil is on top of the pig’s head, then the image is typical; (c) If the veil’s location is different, the image may also be typical.

For example, in Fig. 1a, the pig is not compatible with its context (a bridal veil on its head), and the veil is also not compatible with its context — on a pig’s head. We propose an unsupervised approach by using reconstruction losses of masked regions. We expect that a self-supervised model trained on masked region reconstruction could learn enough implicit knowledge of contextual compatibility; this pre-trained model may then be used to detect atypical images.

Our second hypothesis is that the interactions between objects and their spatial relative positions play a key role in detecting atypicality. If it were a handled brush instead of a bridal veil over the pig’s head (Fig. 1b), or if the veil were placed at another location instead of on top of the pig’s head (Fig. 1c), the image would no longer be atypical. In order to better interpret object-object spatial interaction, we propose a new method to compute the attention weights between key-query regions of our transformer-based models.

Finally, our third hypothesis is that, for some types of persuasive atypicality, the semantic relation between nearby object classes may offer compatibility clues beyond visual features. In Fig. 1a, knowing that there is a “pig” and a “bridal veil” and their spatial relationship may be helpful to conclude that the image is atypical, instead of knowing exactly what that pig or veil look like. To take advantage of

semantic knowledge learned in language models, we fine-tune BERT on detected class labels of regions of interest.

Experiments on a recent visual advertising dataset [48] demonstrate the effectiveness of our approaches and support our hypotheses. Our approach outperforms prior approaches for abnormality detection (e.g. a One-Class SVM) by more than 9%. We have also gleaned insights on how different types of persuasive atypicality impact the detection performance. We validate that atypicality transformations involving spatial interactions between objects are better solved by our approaches than baselines. Then we evaluate the generalization of our approaches using an existing dataset of real-scene, non-persuasive atypical images [46].

To understand the labelling requirement of both tasks, we compare our unsupervised approaches of contextual compatibility with supervised models which are trained on the ground-truth labels. We observe very different performances on the two datasets, which reveals that the labelling requirement depends on the training size ratio between supervised and unsupervised methods and the complexity of the atypicality transformations. Lastly, we investigate two possibilities for representing the image context: visual compatibility versus semantic compatibility. Experimental results show that visual features are essential, but the semantic compatibility can help when atypicality transformations feature unusual combination of normal objects.

2. Related Work

To set our work, which focuses on images with persuasive intent, in the context of the broader atypicality detection literature, we present an overview of prior efforts. Moreover, because our approach for capturing spatial relationships is based on self-attention, we also review related work on transformers and self-attention in computer vision, as well as self-supervised learning through masking.

Atypicality Detection. Prior work focuses on detecting atypical objects in real-world images. Bergmann *et al.* develop unsupervised methods for detecting diverse defects such as scratches, dents, contaminations, and structural changes [4]. Wang *et al.* detect atypical objects through Gaussian Process models based on the distribution of object detection scores in different regions of interest [46]. Choi *et al.* detect out-of-context objects and scenes by a graphical model and show that physical support relationships between objects are an important clue [8]. Saleh *et al.* classify anomalies in images in three categories (object-centric, context-centric and scene-centric) and build a generative model from visual attributes in regular images [38]. Most prior studies investigate atypicality that is (1) physically created in the real world, rather than generated with computer graphics; and (2) predominantly accidental and certainly not aiming to convey meaning or persuade an audience to take a certain action. One exception is the work of Ye *et al.* [48] on interpreting the visual rhetoric in ad-

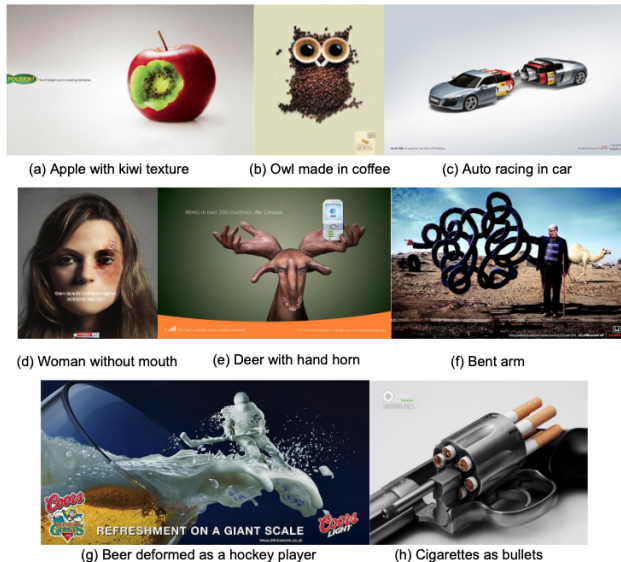


Figure 2. Atypical object transformations in ads; [48]’s dataset.

vertisements. Because ad images are intentionally designed by experts to create an association in viewers’ minds, many atypical objects in their dataset cannot appear in the real world (e.g. a kiwi inside an apple). Moreover, those objects are diverse and not limited to a specific set of categories, as they are in Wang *et al.*’s work [46], in which atypical objects are all from PASCAL VOC [12].

Ye *et al.* devised a taxonomy of atypicality based on object transformations¹ but only supervisedly trained a basic VGG16 model to detect atypicality as a whole, not per category. The eight categories they defined are:

- 1) Texture Replacement 1 (**TR1**): Objects’ texture borrowed from another object, e.g. kiwi inside apple, Fig. 2a.
- 2) Texture Replacement 2 (**TR2**): Texture created by combining several small objects, e.g. owl from beans, 2b.
- 3) Object Inside Object (**OIO**), e.g. auto racing in car, 2c.
- 4) Object w/ Missing Part (**OMP**), woman w/o mouth, 2d.
- 5) Combination of Parts (**CP**): Object composed by parts from different objects, e.g. deer head with hand horn, 2e.
- 6) Solid Deformed Object (**SDO**), e.g. human arm bent, 2f.
- 7) Liquid Deformed Object (**LDO**), e.g. beer as player, 2g.
- 8) Object Replacement (**OR**): The whole object appearing in the context normally associated with another, e.g. cigarettes placed in the context where bullets occur, 2h.

Our work closely examines the relationship between our proposed models and each persuasive atypicality category.

Transformers in Computer Vision. Transformers were first introduced by Vaswani *et al.* as a new network architecture based on attention mechanisms for machine translation [44]. Transformers can perform a variety of tasks by computing scores solely based on self-attention layers,

¹https://people.cs.pitt.edu/~nhonarvar/data_analysis/interface.html

without the need for expensive and non-parallelizable recurrence. Recently, transformers have been demonstrated as an effective architecture in many problems in natural language processing [9, 34], speech processing [25, 42], computer vision [30, 6, 11] and vision-language tasks [43, 24, 20, 40, 50, 32, 22, 7]. Since the transformer architecture is permutation-invariant, a positional encoding is necessary to provide the order information of the sequential input. For work which represents the image by a set of regions of interest, a common way is to embed the bounding-box coordinates of each region and potentially the fraction of image area covered [7, 43, 24]. For pixel-level representation, Carion *et al.* explore sinusoidal embeddings based on the absolute position and a learnt positional encoding of pixels [6]. However, experimentation in machine translation [39] and music generation [16] suggested that using relative positional embeddings results in significantly better accuracy. Adding the absolute positional encoding to the inputs, as done in [11, 6, 43], is not always sufficient. Explicitly modeling relative position information separately from other inputs (e.g. features) extends the self-attention mechanism to efficiently consider spatial relationship between each query-key pair [39, 35, 3, 51]. Ramachandran *et al.* [35] and Bello *et al.* [3] define 2D relative position embeddings by the relative distance between the position of the query and key pixel. Our approach follows the idea of Ramachandran *et al.* except that our relative position embedding is at the region level. Our objective is to model spatial relationships between *objects*, thus a pixel-level representation does not make sense. Besides, we can add overlapping area information to the relative spatial feature between two regions, which a pixel-level representation cannot. Kant *et al.* also consider relative spatial relationship between object regions, but they transform spatial relationship into twelve categories and then apply the adjacency matrices as an additional attention mask on their base model architecture [17]. Therefore, they only consider the relative spatial direction and ignore the concrete relative distance between pairwise objects, which loses essential information compared to our method. Another weakness is their spatial relationship categories do not have full coverage, e.g. the spatial relationship between two non-overlapped objects far from each other is ignored. We are not aware of any prior work that performs atypicality detection with any type of transformer, nor with the relative-spatial transformer we propose.

Self-supervised Learning. Self-supervised learning through masked or next-token prediction is a commonly-used method for language modeling in natural language processing [9, 34]. In computer vision, methods exist to learn visual representations through pretext tasks, e.g. via colorization [49, 19, 45], jigsaw puzzles [29, 10], inpainting [31], instance discrimination [47], or even pretext-invariant objectives [26]. Prior work demonstrates the effectiveness

of these visual representations for transfer learning [13]. Representations can also be learned by predicting context in a multi-modal setting [43, 24, 41, 5, 27]. Our work follows Tan *et al.*'s method by using masked object feature regression for learning visual representations [43], but Tan *et al.* operate in a cross-modal setting, while we operate in a visual one. To our knowledge, we are the first to use self-supervised learning based on context prediction for detecting image atypicality.

3. Approach

We define atypicality detection as a binary classification task: for a given image I , our model aims to predict whether I is atypical or not. We first present our unsupervised atypicality detection system, which leverages masked region reconstruction as the pretext task, and learns implicit knowledge of contextual compatibility from large-scale unlabeled data. The reconstruction losses of masked regions are the clue for predicting atypicality of a test image. We then introduce our Relative-Spatial Transformer which extends the self-attention layer to explicitly model relative position information separately from visual features.

3.1. Masked Region Reconstruction

Fig. 3a shows an overview of our approach. An image I is represented by a set of regions $R = \{(v_1, p_1), (v_2, p_2), \dots, (v_n, p_n)\}$, where v_i could be region i 's visual feature vector, pixel matrix, class labels, etc., and p_i is the positional information. Our hypothesis is that if an image is atypical, the objects appearing in it would not be compatible with each other, thus it would be hard to reconstruct a masked region from image context. We first pre-train a model to reconstruct a region from context using normal cases, then use it to detect atypicality in new test images.

For the pre-training process, we take inspiration from masked language modeling (e.g. BERT [9]) and cross-modality representation learning (e.g. LXMERT [43]). The model is trained to reconstruct the masked regions given the remaining regions, on many general, normal images (which could potentially contain a small proportion of atypical cases). Different from BERT or LXMERT, which aims to learn a language or visual-language representation, our model aims to learn the common co-occurrences and typical spatial relationship between objects.

At test time, we mask each region in the image and compute the reconstruction loss. We compute the average loss of all regions as a clue for predicting atypicality. We use average rather than maximum loss because if an image is atypical, the masked region reconstruction loss is high not only when an atypical object is masked, but also when its surrounding object is masked since it is also hard to reconstruct a normal object from an atypical context.

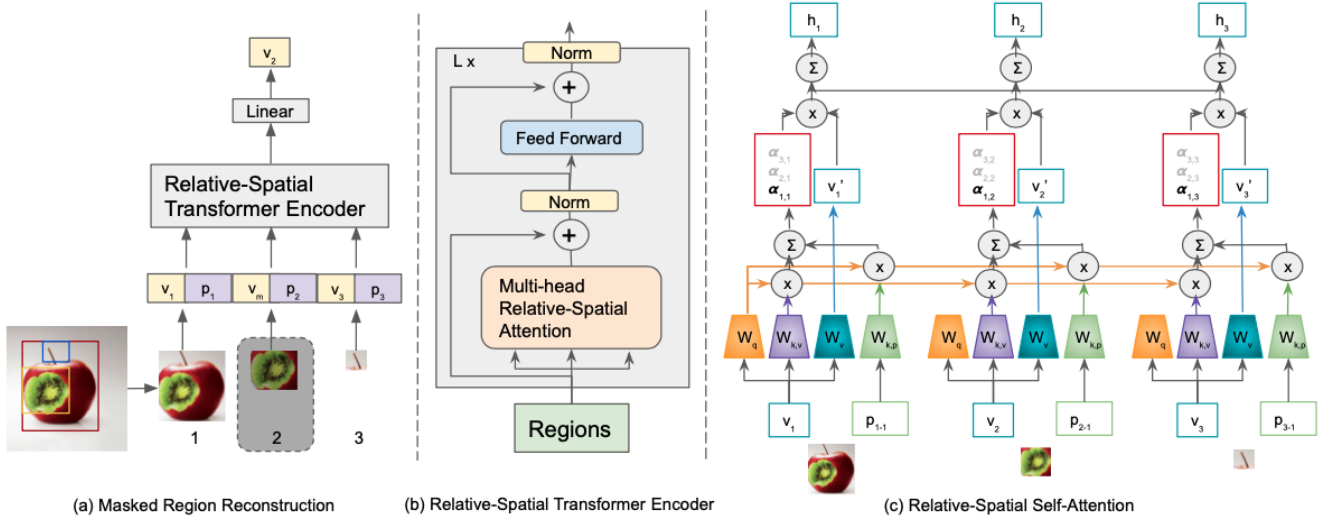


Figure 3. Model overview. (a) A set of regions extracted from the image are the input to the Relative-Spatial Transformer Encoder. The model is trained for reconstructing the visual feature of the masked region 2. (b) The architecture of Relative-Spatial Transformer Encoder. The key difference from the standard transformer Encoder is the attention computation. (c) The mechanism for computing Relative-Spatial Self-Attention. This scheme shows the case when region 1 is the query.

3.2. Relative-Spatial Transformer

Our model extends the transformer architecture [44]. A common input representation to a transformer for computer vision tasks is the summation of the visual embedding and the positional embedding of the region [6, 43, 11]. However, this technique has two weaknesses. First, when computing attention weights with these input vectors, the visual feature and positional information share the same projection weight without any distinction, therefore the model cannot flexibly adjust the importance of region visual and position. Second, the positional embedding represents the absolute coordinate of the region, however, it is the *relative* spatial relationship between the masked and the context region which matters for detecting atypicality (e.g. is the veil above or below the pig?). In order to overcome both weaknesses, we propose the Relative-Spatial Transformer which (1) computes the visual-visual interaction and visual-position interaction separately, and (2) is shift-invariant, similar to convolutions but unlike a standard transformer.

The Relative-Spatial Transformer (RST) follows the same architecture as the transformer (T) of [44] except for a new way for computing the multi-head self-attention layer, as shown in Fig. 3. The attention weight of the query region i and key region j is computed as:

$$A_{i,j}^{rel} = V_i^T W_q^T W_{k,V} V_j + V_i^T W_q^T W_{k,P} P_{j-i} \quad (1)$$

where V_i and V_j are visual features of regions i and j ; W_q is the projection weight of the query region visual feature; $W_{k,V}$ and $W_{k,P}$ are respectively the key region's projection weights of visual features and relative positions; and P_{j-i} is the relative position of region j with respect to region i . The first term computes the interaction between the query

and key visual content; the second term computes the interaction between the query visual content and the relative position of the key region. The summation of both terms shows the importance of the key region to the query region. Then we compute the normalized attention weight $\alpha_{i,j}^{rel}$ as a softmax layer over $A_{i,j}^{rel}$ for all possible key regions. The last hidden layer of region i is computed as:

$$h_i = \sum_j \alpha_{i,j}^{rel} W_v V_j \quad (2)$$

where W_v projects the value region's visual feature.

The reconstruction loss of the masked region i is computed as the mean squared error (i.e. squared L2 norm) between the input visual feature v_i and the last hidden layer h_i of the encoder:

$$L_i = \|v_i - h_i\|_2^2 \quad (3)$$

For computing the relative position of j with respect to i , we compute the x-axis and y-axis distance of the top-left and bottom-right corners of the two bounding boxes:

$$P_{j-i} = [x_j^l - x_i^l, y_j^t - y_i^t, x_j^r - x_i^r, y_j^b - y_i^b] \quad (4)$$

where (x_i^l, y_i^t) is the coordinate of the left-top corner of region i , (x_i^r, y_i^b) is the coordinate of the right-bottom corner of region i ; similarly with region j . We also explore adding Intersection-over-Union area between region i and j as an additional relative positional feature.

4. Experiments

In the subsequent experiments, we first evaluate our contextual compatibility modeling approach on the intent- and persuasion-driven atypicality in the Ads dataset [48]. Our

experiments show that Relative-Spatial Attention leads to an improvement across a diverse array of atypicality sub-categories. Then we test the generalization of our approach on real-world, non-persuasive atypical images, by detecting atypicality within each object class, on a dataset we refer to as the Single-Object dataset [46]. To understand the labelling requirement of each task, we compare our unsupervised contextual compatibility approaches with supervised models trained on the atypical/typical labels. When considering the different possibilities for representing the image context, we compare visual versus semantic compatibility.

4.1. Setup

Input Representations. We use Faster R-CNN [36] pre-trained on Visual Genome [18] for extracting the visual features [2]. Faster R-CNN itself uses ResNet-101 [14] pre-trained for classification on ImageNet [37]. We take the features of each detected object as the visual representation of the corresponding region. We select a fixed number of objects (36) by sorting detections by confidence score. Each region is represented by its bounding-box coordinates and its 2048-dimensional region-of-interest (RoI) features.

Self-supervised Training and Testing. Following BERT [9], we mask 15% of regions in each sequence at random during training. All masked regions are replaced by a trainable vector with the same dimension as the RoI feature. The spatial information of the masked region is given. We use a batch size of 128 and train for 20 epochs with learning rate of $1e-3$. For testing, we mask one region with the learned vector at a time, then compute the average reconstruction loss of all regions. The higher the loss, the more likely the image is atypical. We compute the ROC-AUC score as the evaluation metric since it measures model performance across all possible classification thresholds, by reporting the probability the model ranks a random atypical example higher than a random typical one.

Model Size. We denote the number of layers (*i.e.*, transformer blocks) as L , the hidden size as H , and the number of self-attention heads as A . We primarily report results on the model with $L=1$, $H=768$, $A=8^2$.

Baseline Models. We consider two baselines, Auto-encoder and One-Class SVM, since they are standard methods for detecting abnormality and outliers [1, 21]. For the **Auto-encoder**, we implement the same encoder as DCGAN’s discriminator and DCGAN’s generator as the decoder [33], using the hyperparameters in [33]. The loss is L2 error between input and generated images. However, we make an interesting observation that atypicality relates to image complexity in a potentially counter-intuitive way: We found strong correlation between atypical images and

²There are no extra trainable parameters in RST compared to T. In Fig. 3c, $W_{k,v}$ is extra parameters of size of $d_p * d_v$ (dimensions of position p & visual v vectors), but unlike RST, T requires trainable parameters of size $d_p * d_v$ for projecting p to the same dimension as v for the summation.

relatively plain backgrounds, likely because ad designers of atypical images want to make sure the image is plain enough for the audience to notice the atypicality. Images with uniform background are more easily reconstructed while images with plenty of objects are harder. Further, images with more pixels tend to contain more information to be compressed and reconstructed. To ensure the auto-encoder captures atypicality rather than complexity, we need to normalize for image complexity. We first preprocess all images by resizing them to a fixed number of pixels ($64*64$). We also measure image complexity (IC) as the average of horizontal and vertical gradient of pixels ($IC = avg(I_x^2 + I_y^2)$ where I_x and I_y are respectively the horizontal and vertical gradient). Then we divide the auto-encoder reconstruction loss by IC . In addition, to force the auto-encoder model to learn an effective encoder and decoder, we limit the dimension of the middle hidden layer to 2048 which is much smaller than the input image dimension ($3*64*64$). For the **One-Class SVM** model, we represent each image by the average of its 36 RoI feature vectors. Then we fit the One-Class SVM model³ with default settings on the training images.

4.2. Unsupervised persuasive atypicality detection

Data. We evaluate our method on a dataset of advertisement images where atypicality is creative and has a purpose to convince an audience to take a certain action [48]. The Ads dataset contains in total 64,832 ad images and the authors annotated 3,928 of them for the atypicality task. Since each image is annotated by one or multiple annotators, we set a rule for deciding the atypical/typical label if annotators do not agree with each other. In particular, we consider an ad atypical if any annotator labels it as atypical. We use the *ifany* rule because some atypical cases are subtle, subjective or need background knowledge, thus any annotator providing the atypical label is cause to believe the image is not quite typical. Under this labeling rule, there are 2,285 atypical ads and 1,643 typical ads. For the self-supervised training, we use all ads except for those 3,928 with atypicality labels. For supervised training and for testing, we randomly split the 3,928 atypical/typical images using a 7:1:2 ratio for train:val:test sets. Note we did not use any training data from the atypicality dataset for our unsupervised methods, to make them fairly comparable to supervised methods. All methods are evaluated on the exact same test set.

Results. The experimental results of our unsupervised contextual compatibility approaches are shown in the upper part (*unsup*) of Tab. 1. To gain insights on the impact of different types of persuasive atypicality on the detection result, we also report the model performance on the eight atypicality categories separately, as defined in the Ads dataset (Sec. 2). Experimental results in Tab. 1 show that our approaches significantly outperform baseline models overall (MICRO AVE) and for CP, OR, Others (with p-

³<https://scikit-learn.org/stable/modules/generated/sklearn.svm.OneClassSVM>

| | Methods | TR1 | TR2 | OIO | OMP | CP | SDO | LDO | OR | Others | MICRO AVE |
|-------|-----------------------|--------------|--------------|--------------|--------------|--------------|--------------|--------------|--------------|--------------|--------------|
| unsup | Auto-encoder | 54.67 | 63.28 | 38.79 | 52.98 | 57.78 | 56.62 | 56.05 | 48.57 | 50.99 | 52.52 |
| | One-Class SVM | 64.81 | 68.27 | 59.36 | 65.81 | 54.21 | 65.12 | 54.43 | 56.31 | 54.23 | 58.82 |
| | Transformer (ours) | 62.66 | 60.72 | 63.07 | 42.52 | 69.18 | 63.71 | 61.63 | 64.05 | 63.68 | 62.86 |
| | RS Transformer (ours) | 67.50 | 68.37 | 67.31 | 55.18 | 71.26 | 68.67 | 63.99 | 61.84 | 59.68 | 64.32 |
| sup | RoI Feature only | 66.40 | 65.80 | 60.13 | 56.82 | 63.77 | 67.41 | 62.67 | 62.98 | 59.41 | 62.85 |
| | Transformer | 66.11 | 63.16 | 63.37 | 64.07 | 66.55 | 71.58 | 70.21 | 66.03 | 62.21 | 65.58 |
| | RS Transformer | 65.56 | 64.00 | 62.20 | 53.43 | 70.80 | 71.11 | 75.37 | 67.07 | 65.59 | 66.75 |

Table 1. Experimental results on the Ads dataset. AUC scores for each atypicality category and the micro average are reported.

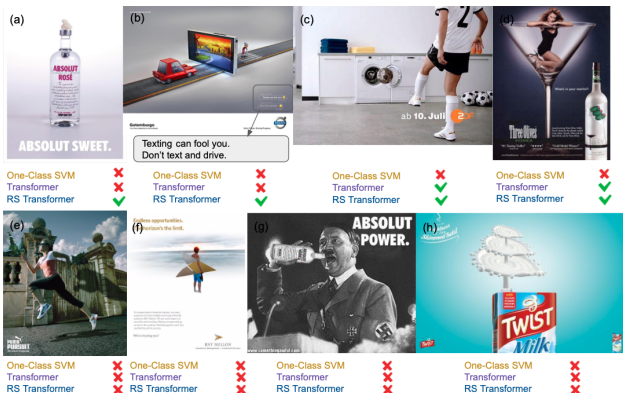


Figure 4. Detection results by the baseline and our models for selected images from the Ads dataset.

value < 0.1).⁴ While Transformer (T) is an existing architecture, and Relative-Spatial Transformer (RST) is our new design, neither has been used for atypicality detection before. T outperforms the simpler baselines significantly, but RST achieves the best results overall. By looking into each category, RST leads to an improvement across a diverse array of atypicality types. In particular, the improvement of RST over T is large for TR1, TR2 and OIO where atypicality mainly comes from unusual spatial relationship between normal objects (these categories involve object compositions). These results demonstrate that our approach of checking for contextual compatibility is effective for detecting persuasive atypicality and our proposed RST architecture does capture object-object spatial relationships well. OMP is the only atypicality category for which the baseline model (One-Class SVM) is better than ours. This is because this type of atypicality only comes from a single object without any complex interaction with surrounding objects.

Error analysis. We qualitatively show several cases where the One-Class SVM fails (Fig. 4a - d) or both the baseline and our models fail (Fig. 4e - h). One-Class SVM fails when atypicality involves composition of normal objects (e.g., cream on top of alcohol bottle), while our transformer models (especially RST) detect this atypicality by learning context via self-supervised training and show large

⁴Details on the significance tests are in the supplementary file.

| | Methods | MICRO AVE |
|-------|---------------------------|--------------|
| unsup | Transformer - L1 | 62.86 |
| | Transformer - L4 | 64.14 |
| | RS Transformer - L1 | 64.32 |
| | RS Transformer - L4 | 64.39 |
| | RS Transformer - L1 - IoU | 64.99 |

Table 2. Ablation study of layer number of encoder and relative positional feature. The micro average AUC scores are reported.

gains. However, our model fails to capture metaphoric similarity: Fig. 4e and 4f look typical at first, but shade versus puma, surfboard versus brand make them atypical. It also fails to interpret symbolic meanings: vodka is held like a microphone by Hitler who is a symbol of power in Fig. 4g. Thus, typicality judgment requires more fine-grained visual features, and knowledge of historical figures.

Ablation. To see the impact of the number of transformer blocks (model depth), we conduct an ablation study on the layer number (L). Considering the variation of relation position features, we add an additional feature, Intersection-over-Union area (IoU), to the previous relative coordinates. Results are shown in Tab. 2. We find that the deeper Transformer greatly improves over a shallow Transformer, while Relative-Spatial Transformers are less sensitive to depth. In addition, we observe that a shallow RS Transformer is competitive against a deep Transformer, suggesting that the proposed RS Transformer is more efficient. We also observe that adding the area overlap (IoU) feature slightly improves performance.

4.3. Performance on non-persuasive atypicality

Data. We investigate how our approach generalizes to non-persuasive atypicality, where the unusual object itself is the main source of atypicality and there is no need to consider the complex spatial relationship between objects for predicting atypicality. For answering this question, we use Wang *et al.*'s Single-Object dataset [46] for evaluation. Their dataset contains 20,420 regular/unusual images belonging to 20 classes. Different from the Ads dataset with various atypicality transformations, each image in the Single-Object dataset has only one main object which is atypical or not.

Definition. Let C denote a given object category, with $C = C^r \cup C^u$ and $C^r \cap C^u = \emptyset$, where C^r and C^u respec-

| Methods | | aeroplane | apple | bicycle | boat | building | bus | car | chair | cow | dining table |
|---------|------------|-------------|-------------|-------------|-------------|-------------|-------------|-------------|-------------|-------------|--------------|
| unsup | AE | 0.74 | 0.44 | 0.58 | 0.78 | 0.85 | 0.55 | 0.74 | 0.52 | 0.52 | 0.33 |
| | T (ours) | 0.93 | 0.86 | 0.84 | 0.90 | 0.86 | 0.86 | 0.92 | 0.78 | 0.74 | 0.90 |
| | RST (ours) | 0.90 | 0.78 | 0.76 | 0.88 | 0.83 | 0.78 | 0.87 | 0.70 | 0.65 | 0.82 |
| sup | T (ours) | 0.99 | 0.96 | 0.99 | 0.98 | 0.95 | 0.99 | 0.99 | 0.98 | 0.99 | 0.93 |
| | RST (ours) | 1.00 | 0.99 | 0.96 | 0.99 | 1.00 | 0.99 | 1.00 | 0.95 | 0.97 | 0.99 |

| Methods | | horse | house | motorbike | road | shoes | sofa | street | table lamp | train | tree | mAP |
|---------|------------|-------------|-------------|-------------|-------------|-------------|-------------|-------------|-------------|-------------|-------------|-------------|
| unsup | AE | 0.42 | 0.65 | 0.40 | 0.65 | 0.71 | 0.64 | 0.59 | 0.39 | 0.45 | 0.56 | 0.58 |
| | T (ours) | 0.80 | 0.90 | 0.71 | 0.91 | 0.87 | 0.83 | 0.90 | 0.82 | 0.77 | 0.80 | 0.85 |
| | RST (ours) | 0.75 | 0.90 | 0.60 | 0.85 | 0.76 | 0.75 | 0.90 | 0.62 | 0.67 | 0.74 | 0.78 |
| sup | T (ours) | 1.00 | 1.00 | 0.96 | 0.99 | 0.98 | 0.92 | 1.00 | 0.92 | 1.00 | 1.00 | 0.98 |
| | RST (ours) | 0.95 | 1.00 | 0.93 | 0.97 | 1.00 | 0.89 | 1.00 | 0.92 | 0.96 | 1.00 | 0.97 |

Table 3. Experimental results on the Single-Object dataset. Average Precision for each class and the macro average (mAP) are reported.

tively means the set of regular images or unusual images in category C . The task is to determine, for any test image $I \in C$, whether $I \in C^u$. In other words, our task is to detect atypical images from each single object class. This is different from Wang *et al.*'s [46] problem setting: their task aims to determine, for any test image $I \in C \cup O^r$ (with O^r denoting regular images not containing the object in category C), if $I \in C^u$. We formulate the task in a different way because our focus is to evaluate our methods on atypicality detection within a single object class and we only use C^r as our training data. In contrast, [46] also train object detectors on $C^r \cup O^r$ then use the object detection scores for predicting atypicality in C . In conclusion, our method performance is not directly comparable to theirs since neither our training nor test set includes O^r .

We use the Auto-encoder model as a baseline. Given that each image only contains one main object, we do not normalize the auto-encoder loss with image complexity as we did for the Ads Dataset. We follow the same split as Wang *et al.*, dividing C^r into training (C_{train}^r) and test set (C_{test}^r). For each object category C , our models and the baseline are trained on C_{train}^r and evaluated on $C^u \cup C_{test}^r$.

The upper part (*unsup*) of Tab. 3 shows the results. We use the same evaluation metric, Average Precision, as Wang *et al.* Different from what we observe with the Ads dataset, Transformer is generally more effective than the RS Transformer here. The reason is that RST does not capture useful information for predicting atypicality since the Single-Object dataset has little object-object spatial relationship as the atypicality source. Moreover, some learnt interactions between objects by RST might be noisy because of overfitting with only hundreds of training samples (as shown in Tab. 4). For this task, a standard attention mechanism with regions' absolute position as input can handle those single atypical objects well, and Transformer achieves comparable results to those shown in [46] (mAP of 0.90).⁵ In conclu-

⁵Even though they are not directly comparable, the inclusion of these earlier results is still informative because we aimed to show our approach produces results in the same ballpark.

| Methods | Ads | aeroplane | apple | bicycle |
|--------------|--------|-----------|-------|---------|
| Unsupervised | 46,757 | 169 | 667 | 268 |
| Supervised | 2,741 | 189 | 429 | 312 |

Table 4. Training size for unsupervised and supervised models.

sion, our unsupervised approach by checking for contextual compatibility works well not only on persuasively creative images with complex atypicality transformation, but also on single-object images. As expected, RST is not beneficial for detecting non-persuasive atypicality of single object.

4.4. Are supervised labels essential for these tasks?

Models. To understand the labelling requirement for detecting atypicality, we compare our unsupervised contextual compatibility approaches with supervised models trained on the atypical/not labels, for both Ads and Single-Object. We use the same Transformer and RS Transformer architectures for fair comparison. We also add a supervised baseline model which is trained only on the RoI features (each image is represented by the average of all regions-of-interest features).⁶ For transformers, the output layer is an average pooling over the last hidden layer followed by a simple 2-layer neural network for predicting the atypicality label. For the RoI baseline, the input image features feed directly to the output layer which is the same 2-layer network.

Results. Tab. 1 and Tab. 3 show the comparison of unsupervised and supervised approaches for the Ads and Single-Object datasets, respectively. We find that for Ads, our unsupervised approaches achieve comparable performance to the supervised approaches, which highlights that even with labeling the task is still difficult. This also demonstrates the effectiveness of our proposed contextual compatibility method. When looking into each atypicality category, we observe the unsupervised RS Transformer wins on those atypicality transformations which involve more object-object interaction, *e.g.* TR1, TR2, OIO, CP. This is expected because RST efficiently learns contextual compat-

⁶The input features are the same as the One-Class SVM baseline. This baseline is conceptually similar to the approach in Ye *et al.* [48] except that they use VGG16 for extracting the image features.

| | Methods | TR1 | TR2 | OIO | OMP | CP | SDO | LDO | OR | Others | MICRO AVE |
|-------|-------------------------|--------------|--------------|--------------|--------------|--------------|--------------|--------------|--------------|--------------|--------------|
| unsup | Transformer with VF | 62.66 | 60.72 | 63.07 | 42.52 | 69.18 | 63.71 | 61.63 | 64.05 | 63.68 | 62.86 |
| | RS Transformer with VF | 67.50 | 68.37 | 67.31 | 55.18 | 71.26 | 68.67 | 63.99 | 61.84 | 59.68 | 64.32 |
| | Transformer with CL | 51.39 | 58.28 | 61.90 | 41.53 | 62.76 | 54.80 | 60.49 | 56.09 | 62.38 | 57.63 |
| | RS Transformer with CL | 54.89 | 62.30 | 60.49 | 47.03 | 61.47 | 58.25 | 53.00 | 58.28 | 61.76 | 58.46 |
| sup | Fine-tuned BERT with CL | 62.94 | 69.59 | 59.02 | 56.25 | 70.74 | 69.87 | 62.00 | 65.96 | 62.30 | 64.71 |

Table 5. Comparison of Faster R-CNN RoI visual feature (VF) and predicted class label (CL). AUC for each atypicality category and micro ave are reported, with best AUC per column bolded. AUC for *Fine-tuned BERT with CL* is bolded if it outperforms all unsup. methods.

ibility knowledge from the large-scale normal images with the RS self-attention mechanism which is designed for precisely modeling spatial relationship between objects. In addition, the RS Transformer outperforms the original Transformer for the supervised setting as well. For the Single-Object dataset shown in Tab. 3, we see the supervised approaches give a nearly-perfect performance, which reveals that providing labels greatly reduces the difficulty of the atypical detection task for single object.

When comparing the performance of unsupervised and supervised approaches, we have different observations on the Ads and Single-Object datasets: for Ads, our unsupervised approaches achieve comparable performance to the supervised ones; for Single-Object, the supervised methods substantially outperform the unsupervised ones. One reason may be that unsupervised models have 20 times more training data for the Ads task, while the training size is similar between unsupervised and supervised methods for Single-Object, as shown in Tab. 4. Another reason may be that for the single-object task, it is easy for models to capture the key features of a normal object from unusual training examples, *e.g.* what does an apple usually look like. However, for more complex atypicality transformation as in Ads, a few labels do not help compared to learning various forms of compatibility through many unlabeled samples.

4.5. Visual versus semantic compatibility

We next consider different possibilities for representing the image context, namely checking visual versus semantic compatibility. Our previous experiments use Faster R-CNN RoI features which represent the visual content of the region and then learn compatibility from them. We now consider using the class labels predicted by Faster R-CNN as the semantic features of the region and then we use the same model for learning semantic compatibility.

Training. For unsupervised training with transformer-based models, the input is a sequence of class labels with the bounding-box coordinates of regions ordered by the detection confidence score. Similarly with visual features, we mask one (or several during the training) object class label by a [MASK] token in the input, and the model is trained to predict the class label of the masked region. We use the cross-entropy loss for training and testing; the loss is the atypicality signal. Since the input of class labels are discrete textual tokens, we project them through an embedding

layer before feeding to the transformer; at the output, we project the last hidden layer of the masked input back to the class label by a decoder which shares the same weight as the embedding layer. We follow the same experimental setting as with the visual features. For supervised training, we fine-tune the pre-trained BERT model (bert-base-uncased)⁷ with the sequence of class labels as input. We use batch size 16, learning rate 3e-5 and 5 epochs, as suggested in [9].

Results. Experimental results on the Ads dataset are shown in Tab. 5. We find that checking semantic compatibility (CL) is not as effective as checking the visual compatibility (VF) under the unsupervised setting. Thus, visual features contain more useful information (*e.g.*, the visual features of an atypical apple and a typical apple are different; however, the class label input does not have this information when the atypical apple is correctly detected as "apple" by Faster R-CNN), and only checking the semantic compatibility is not enough for solving this task. However, fine-tuned BERT with predicted class labels slightly outperforms the unsupervised RS Transformer using visual feature input, especially for those categories whose atypicality transformations are mainly from unusual combination of normal objects, such as TR2 and OR, which are well captured by the semantic compatibility.

5. Conclusion

We have proposed to model contextual compatibility as an unsupervised approach to detect atypicality in persuasive imagery. Our new self-supervised Relative-Spatial Transformer improves the detection performance on a visual advertising dataset, compared to standard baselines and to a novel application of a classic transformer architecture that has not been used for atypicality prediction before. Furthermore, analyses by atypicality categories show that our method is especially effective on atypicality transformations involving spatial interactions between objects.

In the future, we will extend the relative-spatial self-attention mechanism by adding terms capturing relations specific to individual atypicality categories, and we will capture inputs from other modalities, *e.g.* the slogans in ads, to model contextual compatibility more efficiently.

Acknowledgement: This work was supported by National Science Foundation Grant No. 1718262.

⁷https://huggingface.co/transformers/model_doc/bert.html

References

- [1] Jinwon An and Sungzoon Cho. Variational autoencoder based anomaly detection using reconstruction probability. *Special Lecture on IE*, 2(1):1–18, 2015. 5
- [2] Peter Anderson, Xiaodong He, Chris Buehler, Damien Teney, Mark Johnson, Stephen Gould, and Lei Zhang. Bottom-up and top-down attention for image captioning and visual question answering. In *Proceedings of the IEEE/CVF Conference on Computer Vision and Pattern Recognition*, pages 6077–6086, 2018. 5
- [3] Irwan Bello, Barret Zoph, Ashish Vaswani, Jonathon Shlens, and Quoc V Le. Attention augmented convolutional networks. In *Proceedings of the IEEE/CVF International Conference on Computer Vision*, pages 3286–3295, 2019. 3
- [4] Paul Bergmann, Michael Fauser, David Sattlegger, and Carsten Steger. Mvtec ad—a comprehensive real-world dataset for unsupervised anomaly detection. In *Proceedings of the IEEE/CVF Conference on Computer Vision and Pattern Recognition*, pages 9592–9600, 2019. 2
- [5] Gedas Bertasius and Lorenzo Torresani. Cobe: Contextualized object embeddings from narrated instructional video. *Advances in Neural Information Processing Systems*, 33:15133–15145, 2020. 3
- [6] Nicolas Carion, Francisco Massa, Gabriel Synnaeve, Nicolas Usunier, Alexander Kirillov, and Sergey Zagoruyko. End-to-end object detection with transformers. In *European Conference on Computer Vision*, pages 213–229. Springer, 2020. 3, 4
- [7] Yen-Chun Chen, Linjie Li, Licheng Yu, Ahmed El Kholy, Faisal Ahmed, Zhe Gan, Yu Cheng, and Jingjing Liu. Uniter: Universal image-text representation learning. In *European Conference on Computer Vision*, pages 104–120. Springer, 2020. 3
- [8] Myung Jin Choi, Antonio Torralba, and Alan S Willsky. Context models and out-of-context objects. *Pattern Recognition Letters*, 33(7):853–862, 2012. 2
- [9] Jacob Devlin, Ming-Wei Chang, Kenton Lee, and Kristina Toutanova. Bert: Pre-training of deep bidirectional transformers for language understanding. In *Proceedings of the 2019 Conference of the North American Chapter of the Association for Computational Linguistics: Human Language Technologies, Volume 1 (Long and Short Papers)*, pages 4171–4186, 2019. 3, 5, 8
- [10] Carl Doersch, Abhinav Gupta, and Alexei A Efros. Unsupervised visual representation learning by context prediction. In *Proceedings of the IEEE/CVF International Conference on Computer Vision*, pages 1422–1430, 2015. 3
- [11] Alexey Dosovitskiy, Lucas Beyer, Alexander Kolesnikov, Dirk Weissenborn, Xiaohua Zhai, Thomas Unterthiner, Mostafa Dehghani, Matthias Minderer, Georg Heigold, Sylvain Gelly, et al. An image is worth 16x16 words: Transformers for image recognition at scale. In *International Conference on Learning Representations*, 2020. 3, 4
- [12] Mark Everingham, Luc Van Gool, Christopher KI Williams, John Winn, and Andrew Zisserman. The pascal visual object classes (voc) challenge. *International journal of computer vision*, 88(2):303–338, 2010. 2
- [13] Kaiming He, Haoqi Fan, Yuxin Wu, Saining Xie, and Ross Girshick. Momentum contrast for unsupervised visual representation learning. In *Proceedings of the IEEE/CVF Conference on Computer Vision and Pattern Recognition*, pages 9729–9738, 2020. 3
- [14] Kaiming He, Xiangyu Zhang, Shaoqing Ren, and Jian Sun. Deep residual learning for image recognition. In *Proceedings of the IEEE/CVF Conference on Computer Vision and Pattern Recognition*, pages 770–778, 2016. 5
- [15] Nigel Hollis. Why good advertising works (even when you think it doesn't). *The Atlantic*, 31, 2011. 1
- [16] Cheng-Zhi Anna Huang, Ashish Vaswani, Jakob Uszkoreit, Ian Simon, Curtis Hawthorne, Noam Shazeer, Andrew M Dai, Matthew D Hoffman, Monica Dinulescu, and Douglas Eck. Music transformer: Generating music with long-term structure. In *International Conference on Learning Representations*, 2018. 3
- [17] Yash Kant, Dhruv Batra, Peter Anderson, Alex Schwing, Devi Parikh, Jiasen Lu, and Harsh Agrawal. Spatially aware multimodal transformers for textvqa. In *European Conference on Computer Vision*, pages 715–732. Springer, 2020. 3
- [18] Ranjay Krishna, Yuke Zhu, Oliver Groth, Justin Johnson, Kenji Hata, Joshua Kravitz, Stephanie Chen, Yannis Kalantidis, Li-Jia Li, David A Shamma, et al. Visual genome: Connecting language and vision using crowdsourced dense image annotations. *International journal of computer vision*, 123(1):32–73, 2017. 5
- [19] Gustav Larsson, Michael Maire, and Gregory Shakhnarovich. Learning representations for automatic colorization. In *European Conference on Computer Vision*, pages 577–593. Springer, 2016. 3
- [20] Gen Li, Nan Duan, Yuejian Fang, Ming Gong, and Daxin Jiang. Unicoder-vl: A universal encoder for vision and language by cross-modal pre-training. In *Proceedings of the AAAI Conference on Artificial Intelligence*, volume 34, pages 11336–11344, 2020. 3
- [21] Kun-Lun Li, Hou-Kuan Huang, Sheng-Feng Tian, and Wei Xu. Improving one-class svm for anomaly detection. In *Proceedings of the 2003 International Conference on Machine Learning and Cybernetics (IEEE Cat. No. 03EX693)*, volume 5, pages 3077–3081. IEEE, 2003. 5
- [22] Liunian Harold Li, Mark Yatskar, Da Yin, Cho-Jui Hsieh, and Kai-Wei Chang. Visualbert: A simple and performant baseline for vision and language. *arXiv preprint arXiv:1908.03557*, 2019. 3
- [23] Karin Liebhart and Petra Bernhardt. Political storytelling on instagram: Key aspects of alexander van der bellen's successful 2016 presidential election campaign. *Media and Communication*, 5(4):15–25, 2017. 1
- [24] Jiasen Lu, Dhruv Batra, Devi Parikh, and Stefan Lee. Vilbert: Pretraining task-agnostic visiolinguistic representations for vision-and-language tasks. *Advances in Neural Information Processing Systems*, 32:13–23, 2019. 3
- [25] Christoph Lüscher, Eugen Beck, Kazuki Irie, Markus Kitzka, Wilfried Michel, Albert Zeyer, Ralf Schlüter, and Hermann Ney. RWTH ASR Systems for LibriSpeech: Hybrid vs At-

- tention. In *Proc. Interspeech 2019*, pages 231–235, 2019. 3
- [26] Ishan Misra and Laurens van der Maaten. Self-supervised learning of pretext-invariant representations. In *Proceedings of the IEEE/CVF Conference on Computer Vision and Pattern Recognition*, pages 6707–6717, 2020. 3
- [27] Pedro Morgado, Yi Li, and Nuno Vasconcelos. Learning representations from audio-visual spatial alignment. In *NeurIPS*, 2020. 3
- [28] Caroline Lego Munoz and Terri L Towner. The image is the message: Instagram marketing and the 2016 presidential primary season. *Journal of political marketing*, 16(3-4):290–318, 2017. 1
- [29] Mehdi Noroozi and Paolo Favaro. Unsupervised learning of visual representations by solving jigsaw puzzles. In *European Conference on Computer Vision*, pages 69–84. Springer, 2016. 3
- [30] Niki Parmar, Ashish Vaswani, Jakob Uszkoreit, Lukasz Kaiser, Noam Shazeer, Alexander Ku, and Dustin Tran. Image transformer. In *International Conference on Machine Learning*, pages 4055–4064. PMLR, 2018. 3
- [31] Deepak Pathak, Philipp Krahenbuhl, Jeff Donahue, Trevor Darrell, and Alexei A Efros. Context encoders: Feature learning by inpainting. In *Proceedings of the IEEE/CVF Conference on Computer Vision and Pattern Recognition*, pages 2536–2544, 2016. 3
- [32] Di Qi, Lin Su, Jia Song, Edward Cui, Taroon Bharti, and Arun Sacheti. Imagebert: Cross-modal pre-training with large-scale weak-supervised image-text data. *arXiv preprint arXiv:2001.07966*, 2020. 3
- [33] Alec Radford, Luke Metz, and Soumith Chintala. Unsupervised representation learning with deep convolutional generative adversarial networks. *arXiv preprint arXiv:1511.06434*, 2015. 5
- [34] Alec Radford, Jeffrey Wu, Rewon Child, David Luan, Dario Amodei, and Ilya Sutskever. Language models are unsupervised multitask learners. *OpenAI blog*, 1(8):9, 2019. 3
- [35] Prajit Ramachandran, Niki Parmar, Ashish Vaswani, Irwan Bello, Anselm Levskaya, and Jon Shlens. Stand-alone self-attention in vision models. *Advances in Neural Information Processing Systems*, 32, 2019. 3
- [36] Shaoqing Ren, Kaiming He, Ross Girshick, and Jian Sun. Faster r-cnn: Towards real-time object detection with region proposal networks. *Advances in Neural Information Processing Systems*, 28:91–99, 2015. 5
- [37] Olga Russakovsky, Jia Deng, Hao Su, Jonathan Krause, Sanjeev Satheesh, Sean Ma, Zhiheng Huang, Andrej Karpathy, Aditya Khosla, Michael Bernstein, et al. Imagenet large scale visual recognition challenge. *International journal of computer vision*, 115(3):211–252, 2015. 5
- [38] Babak Saleh, Ahmed Elgammal, Jacob Feldman, and Ali Farhadi. Toward a taxonomy and computational models of abnormalities in images. In *Proceedings of the AAAI Conference on Artificial Intelligence*, volume 30, 2016. 2
- [39] Peter Shaw, Jakob Uszkoreit, and Ashish Vaswani. Self-attention with relative position representations. In *Proceedings of the 2018 Conference of the North American Chapter of the Association for Computational Linguistics: Human Language Technologies, Volume 2 (Short Papers)*, pages 464–468, 2018. 3
- [40] Weijie Su, Xizhou Zhu, Yue Cao, Bin Li, Lewei Lu, Furu Wei, and Jifeng Dai. Vi-bert: Pre-training of generic visual-linguistic representations. In *International Conference on Learning Representations*, 2019. 3
- [41] Chen Sun, Austin Myers, Carl Vondrick, Kevin Murphy, and Cordelia Schmid. Videobert: A joint model for video and language representation learning. In *Proceedings of the IEEE/CVF International Conference on Computer Vision*, pages 7464–7473, 2019. 3
- [42] Gabriel Synnaeve, Qiantong Xu, Jacob Kahn, Tatiana Likhomanenko, Edouard Grave, Vineel Pratap, Anuroop Sriram, Vitaliy Liptchinsky, and Ronan Collobert. End-to-end asr: from supervised to semi-supervised learning with modern architectures. In *Workshop on Self-supervision in Audio and Speech (SAS) at the 37th International Conference on Machine Learning*, 2020. 3
- [43] Hao Tan and Mohit Bansal. Lxmert: Learning cross-modality encoder representations from transformers. In *Proceedings of the 2019 Conference on Empirical Methods in Natural Language Processing and the 9th International Joint Conference on Natural Language Processing*, pages 5103–5114, 2019. 3, 4
- [44] Ashish Vaswani, Noam Shazeer, Niki Parmar, Jakob Uszkoreit, Llion Jones, Aidan N Gomez, Łukasz Kaiser, and Illia Polosukhin. Attention is all you need. In *Advances in Neural Information Processing Systems*, pages 5998–6008, 2017. 2, 4
- [45] Carl Vondrick, Abhinav Shrivastava, Alireza Fathi, Sergio Guadarrama, and Kevin Murphy. Tracking emerges by coloring videos. In *European Conference on Computer Vision*, pages 391–408. Springer, 2018. 3
- [46] Peng Wang, Lingqiao Liu, Chunhua Shen, Zi Huang, Anton van den Hengel, and Heng Tao Shen. What’s wrong with that object? identifying images of unusual objects by modelling the detection score distribution. In *Proceedings of the IEEE/CVF Conference on Computer Vision and Pattern Recognition*, pages 1573–1581, 2016. 2, 5, 6, 7
- [47] Zhirong Wu, Yuanjun Xiong, Stella X Yu, and Dahua Lin. Unsupervised feature learning via non-parametric instance discrimination. In *Proceedings of the IEEE/CVF Conference on Computer Vision and Pattern Recognition*, pages 3733–3742, 2018. 3
- [48] Keren Ye, Narges Honarvar Nazari, James Hahn, Zaeem Hussain, Mingda Zhang, and Adriana Kovashka. Interpreting the rhetoric of visual advertisements. *IEEE transactions on pattern analysis and machine intelligence*, 2019. 1, 2, 4, 5, 7
- [49] Richard Zhang, Phillip Isola, and Alexei A Efros. Colorful image colorization. In *European Conference on Computer Vision*, pages 649–666. Springer, 2016. 3
- [50] Luowei Zhou, Hamid Palangi, Lei Zhang, Houdong Hu, Jason Corso, and Jianfeng Gao. Unified vision-language pre-training for image captioning and vqa. In *Proceedings of the AAAI Conference on Artificial Intelligence*, volume 34, pages 13041–13049, 2020. 3

- [51] Xizhou Zhu, Dazhi Cheng, Zheng Zhang, Stephen Lin, and Jifeng Dai. An empirical study of spatial attention mechanisms in deep networks. In *Proceedings of the IEEE/CVF International Conference on Computer Vision*, pages 6688–6697, 2019. [3](#)